Activity of Platinum−Gold Alloys for Glucose Electrooxidation in Biofuel Cells

A. Habrioux,[†] E. Sibert,[†] K. Servat,[†] W. Vogel,[‡] K. B. Kokoh,*[,†] and N. Alonso-Vante*[,†]

Laboratory of Electrocatalysis, UMR 6503 CNRS, University of Poitiers, 40 Avenue du Recteur Pineau 86022 Poitiers Cedex, France, and Fritz-Haber-Institut der Max-Planck-Gesellschaft, Faradayweg 4-6, 14195 Berlin, Germany

Received: March 13, 2007; In Final Form: May 18, 2007

Carbon supported Pt−Au catalysts with different bimetallic compositions were prepared by water in oil (w/o) microemulsion. Carbon Vulcan XC-72 was added during the synthesis of particles in order to obtain their good dispersion and a mean particle size distribution of 5.02 ± 0.56 nm. Structural characterization was performed using XRD at wide angles (WAXS), which showed that Pt−Au particles exhibited alloy properties. Electrochemical characterization allowed to estimate the surface composition of Pt−Au alloys, which was close to that of the bulk material $Pt_{20}Au_{80}$. This catalyst composition displayed the best catalytic activity in steady-state conditions in comparison with $Pt_{50}Au_{50}$ or Pt and Au alone. Moreover, a Pt−Au/C catalyst with a metal loading of 40 wt % was immobilized onto a carbon porous tube as anode. A membrane-less biofuel cell was tested using laccase/ABTS biocathode in phosphate buffer (pH 5).

Introduction

Advances in nanoscience have created a new direction for development of nanoscale materials and devices for various applications. Biofuel cells have been classified either as a microbial-based or enzymatic fuel cell according to whether the enzymes are located inside of microorganisms or outside of living cells.

As fuel cells, biofuel cells now constitute a proven research domain if one takes into account the number of works achieved these last 10 years.[1−14] Our objective here is not to be controversial on the interest or the performance of one or the other, but simply to propose another type of source of energy that takes into account the best of the two previous systems. The main benefits of enzyme-based cathodes are the capability to reduce O_2 without side-product such as hydrogen peroxide. Conversely, some reports mentioned that glucose oxidase (GOD) was an efficient anode at a pH value different to that of the main biocathodes (laccase).[15−17] Its performance decreases when O_2 crosses over toward the anode where this oxidant can be reduced to H_2O_2, which inhibits the anode enzyme. Moreover, it was reported that glucose oxidation on GOD was a diffusion controlled reaction in steady-state conditions.[13,14]

It is of great interest and a challenge to prepare catalysts with a controlled composition and distribution in the nanoscale range, which can be used as stable anodes of long duration for glucose oxidation. Gold- and platinum-based electrodes are well tested for their activity in several organics electrooxidation reactions.[18−23] Their utilization as anodes in biofuel cells can allow to maintain the biocompatibility of the cell in environmentally friendly applications. There is a continuous effort toward the development of different synthetic methods based on microemulsions[24−30] and colloids[31−34] with the purpose to improve the catalytic activity of electrode materials. Pt−Au bimetallic nanoparticles as anodes were chosen in this investigation in biofuel cells as a source of renewable and sustainable power, for their special catalytic properties for glucose oxidation. Our previous works showed that Pt is the best catalyst in dehydrogenation of the anomeric carbon in C_1-position while Au is well-known for its remarkable activity in the oxidation of aldehydes and hemiacetals.[21−23]

Experimental Section

Chemicals. Hydrogen tetrachloroaurate hydrate ($HAuCl_4$, $3H_2O$, 99.9%, ACS reagent), trisodium citrate (99%, ACS reagent), tannic acid, Nafion, and tetraethyleneglycolmonododecylether (BRIJ 30) were supplied by Sigma-Aldrich. Dipotassium carbonate (K_2CO_3, 99%, pro-analysis) and hexachloroplatinate (H_2PtCl_6, $6H_2O$, 99,9%, ACS reagent) were purchased from Prolabo and Alfa-Aesar, respectively. The oil phase (n-heptane, 99%) and the reducing agent ($NaBH_4$, 99%) were provided by Acros-Organics. Supporting electrolytes were prepared with potassium dihydrogen phosphate (KH_2PO_4, 99.5%, pro-analysis), NaOH (BDH), sodium dihydrogen phosphate monohydrate (NaH_2PO_4, H_2O), and di-sodium hydrogen phosphate (Na_2HPO_4) were supplied by Merck. β-D-glucose (99%, pro-analysis) was also purchased from Merck. For fuel cell test, 2,2′-azino-bis(3-ethylbenzothiazoline-6-sulfonic acid) diammonium salt (ABTS, 99%, HPLC) purchased from Fluka and laccase produced from *Trametes versicolor* (ATCC 32745) were used to construct the biocathode. All the aqueous solutions were prepared using 18.2 MΩ cm Millipore-MilliQ water.

Carbon Toray and Vulcan XC-72 were provided by Electrochem. Inc. and Cabot, respectively. The carbon porous tubes of one centimeter external diameter used for fuel cell tests were a gift from Novasep Orelis-France. They were characterized by an average pore diameter of 3 μm, porosity of 0.17, thickness of 2 mm and inner diameter of 0.6 cm.

Nanoparticle Synthesis. The preparation of nanoscale particles for the anode was carried out by two methods. Gold nanoparticles were prepared according to the procedure described by Slot and Geuze.[31] A 100 mL of solution was prepared

* Corresponding author. Tel.: +3354945-3625. Fax: +3354945-3580. E-mails: nicolas.alonso.vante@univ-poitiers.fr, boniface.kokoh@univ-poitiers.fr.

[†] University of Poitiers.

[‡] Fritz-Haber-Institut. Present address: Dept. of Chemistry, National Central University, Taiwan.

10.1021/jp0720183 CCC: $37.00
Published on Web 08/08/2007

by mixing at 60 °C, an 80 mL of tetrachloroaurate solution (containing 1 mL of 1% $HAuCl_4$ in 79 mL of ultrapure water) and 20 mL of a reducing solution (containing 1 mL of 1% tannic acid, 4 mL of 1% tri sodium citrate, 15 mL of ultrapure water and K_2CO_3 to adjust the pH of the solution between 7.5 and 8). Elsewhere, platinum and gold−platinum bimetallic nanoparticles were synthesized in water-in-oil (w/o) microemulsion of ultrapure water/tetraethyleneglycolmonododecylether/n-heptane.[24,25] The reduction of Pt and Au ions has been performed using sodium borohydride ($NaBH_4$) as reducing agent.[30] The nanoparticles were formed by mixing two microemulsions with the same composition, one containing the precursor salts (H_2PtCl_6 or $HAuCl_4 + H_2PtCl_6$) and the other, the reducing agent. After the formation of Pt and Pt−Au nanoparticles in the microemulsion, an appropriate amount of carbon Vulcan XC-72 was added under constant stirring for 2 h. The supported catalysts were separated, washed several times with acetone and ultrapure water to eliminate excess of surfactant molecules and finally dried in vacuum over silica gel. The advantage of the procedure which consists in the addition of carbon Vulcan is to prevent the agglomeration of particles during elimination of remaining surfactant.

Physicochemical Characterization of the Catalysts. The catalysts were first characterized by Transmission Electron Microscopy (TEM) using a Philips CM 120 microscope to determine the morphology and size distribution of particles. X-ray patterns were obtained with a Guinier powder diffractometer (HUBER), set at the 45° transmission position. A Johansson type Ge monochromator produces a focused monochromatic Cu−$K_{\alpha 1}$ primary beam ($\lambda = 0.15406$ nm). The powder sample was slightly pressed and fixed between two 3 μm polyethylene foils and measured immediately in ambient conditions. A scan of the pure Vulcan support was used for the background correction. The background-corrected patterns were subjected to the usual angular correction for absorption, polarization and geometrical factors, and plotted versus the reciprocal scattering length $b = 2 \sin \theta/\lambda$ (θ, Bragg angle; λ, wavelength). For the analysis of the X-ray data we measured the integral line width (db) versus peak position (b_r) for the first five peaks (Williamson−Hall plot).[35] The line profiles were fitted by Pearson VII functions. Mean crystallite size, mean internal strains, and mean stacking fault densities were obtained from these plots, based on Warren's treatment of defective metals.[36] The method has been used and described in detail in previous papers.[37,38]

Electrochemical Measurements. All the electrochemical experiments were carried out using a computer controlled VoltaLab Potentiostat PGZ 402 Electrochemical Interface (Radiometer Analytical). For cyclic voltammetry and chronoamperometric experiments, the working electrodes were composed of the metal/C catalysts deposited over vitreous carbon (polished to a mirror-finish prior to each experiment) disk of a rotating disk electrode. The experiments were performed in a conventional three-electrodes Pyrex cell (20 mL). $Hg|Hg_2SO_4|K_2SO_4$(sat.) (MSE) and a slab of vitreous carbon were used as reference and counter electrodes, respectively. The reference electrode was separated from the solution by a Luggin−Haber capillary tip. Cyclic voltammetry was used to characterize the catalyst surface area. The Pt active surface area was estimated by obtaining the charge of hydrogen adsorption/desorption region. The active surface area of the gold and Pt−Au electrodes was obtained from the integration of the oxide reduction regions.

Fuel Cell Test. The fuel cell test was carried out in a membrane-less three electrode Pyrex cell (40 mL) filled with a phosphate buffer prepared with NaH_2PO_4, H_2O and Na_2HPO_4 (pH 5.0), which was 0.1 M in D-glucose.[14] The electrolyte was saturated with nitrogen gas. On the one hand, the biocathode was prepared as previously described in ref 14. In short: Laccase was produced from *Trametes versicolor* (ATCC 32745). The bioreactor was inoculated with the obtained pounded mats. Laccase production was induced with 2,5-xylidine (0.2 mM) at the beginning of the culture. Seven-day-old culture liquid was filtered through glass wool to eliminate the mycelium. Extracellular polysaccharides were precipitated with 10% acetone, separated by successive filtrations (final porosity 0.22 μm). The filtrate was concentrated by ultrafiltration (Millipore YM10, cutoff 10000 Da), and laccase was recovered in 20 mM citrate−phosphate buffer (CPB) pH 5.0 by diafiltration using the same membrane. The enzyme was then applied to a DEAE 52 anion exchange column equilibrated in the same buffer. Combined active non-retained fractions were pooled and concentrated by ultrafiltration on YM 30, then dialyzed against 50 mM phosphate buffer at pH 6.8, where the stability of the enzyme is maximal at 4 °C. After addition of glycerol (30% v/v final), this crude preparation of laccase (around 3 mg mL total protein) was aliquoted and stored at −20 °C. The activity of immobilized laccase on the tube was measured by the rate of oxidation of 1 mM $ABTS^{2-}$ in 0.2 M citrate−phosphate buffer pH 3.0 ($V =$ 8 mL) at 30 °C that was circulated through a spectrophotometric cell. The substrate solution was aerated by air bubbling. The increase in absorbance, corresponding to the production rate of $ABTS^{2-}$ oxidation product, was followed by spectrophotometry at 420 nm ($\epsilon_{420} = 36000$ mol $cm^{-1}L^{-1}$). GOx catalyzed the oxidation of β-D-glucose to gluconic acid, concomitant with the reduction of oxygen to hydrogen peroxide. H_2O_2 was then oxidized using peroxidise in the presence of $ABTS^{2-}$ so as to produce water and $ABTS^{\bullet -}$. The activity of immobilized GOx on the tube was measured by the rate of oxidation of 1.7 mM $ABTS^{2-}$ in the presence of 3.4 U mL^{-1} peroxidase at 30 °C in 0.1 M phosphate buffer pH 7.0 ($V = 4.92$ mL) that was circulated through a spectrophotometric cell. The reaction was started with the addition of 817 μL of 1.1 M glucose solution. For both enzyme assays, the amount of enzyme generating 1 μmol of product over 1 min was taken as one unit (U) of activity. The activity of immobilized laccase on the porous carbon tube was equal to 27 mU cm^{-2}.

Enzyme activity is expressed in terms of enzymatic units (U). One enzymatic unit is the amount of enzyme required to transform 1 μmol of substrate per minute. On the other hand, the anode is prepared with a deposit of the ink containing Pt−Au (1:4) on a carbon porous tube. The two modified carbon tubes were electrically connected to a copper wire. A KCl saturated calomel electrode (SCE) was used as reference. The reference electrode was separated from the solution by a Luggin−Haber capillary tip. An oxygen saturated solution circulated in the inner part of the biocathode compartment. The temperature of the biofuelcell was thermostatically controlled.

Results and Discussion

Physical Characterization. Various powder samples of Pt, Au and Pt−Au catalysts supported on Vulcan XC-72 carbon black were studied by TEM and WAXS analyses. Figure 1 shows a TEM image (a) and the particle size distribution (b) deduced for $Pt_{20}Au_{80}$ catalyst. Assuming a Gaussian distribution, a mean size and dispersion could be obtained for all catalysts, as reported in Table 1 in column 2.

Structure Analysis of Pt−Au Alloys. Wide-angle X-ray scattering pattern (WAXS) experiments were carried out in order to characterize the microstructure of the bimetallic catalyst of

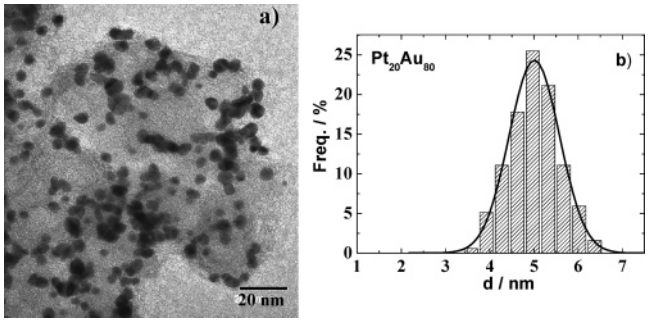

Figure 1. TEM image (a) and histogram of particle size distribution (b), deduced from TEM image. $Pt_{20}Au_{80}$/C catalyst synthesized by w/o emulsion.

TABLE 1: Structural Parameters of Pt−Au Catalysts Obtained from Physical and Electrochemical Characterizations

catalyst	d_{TEM} (nm)	d_{WAXS} (nm)	bulk composition (WAXS) % at. Au	bulk composition (WAXS) % at. Pt	surface composition % at. Au	surface composition % at. Pt
Au	5.05 ± 0.61		(100)			
$Au_{80}Pt_{20}$	5.02 ± 0.56	5.1	80	20	74.1	25.9
$Au_{50}Pt_{50}$	2.80 ± 0.46	3.6	65	35	18.4	81.6
Pt	3.09 ± 0.46			(100)		

the 40% metal loading $Pt_{50}Au_{50}$ and $Pt_{20}Au_{80}$ catalysts. Figure 2 shows the corrected pattern of the $Pt_{20}Au_{80}$ catalyst and the fitted profile (solid line). The fit with five Pearson VII functions gives two important parameters: the accurate peak positions b_r and the integral line width *db* in reciprocal b-space. They are plotted in Figure 3 (full circles). There are large variations of the integral line width that are not expected for simple size broadening. Metal nanoparticles can have large internal strains, varying with the lattice direction represented by the *hkl*-indices according to the elastic anisotropy. Moreover, they are frequently faulted by departing from the regular stacking periodicity ABCABC, described by a stacking fault probability. In previous papers[36−38] we have shown that such line width fluctuations can be ascribed to these defects: as a result of the best fit (open circles in Figure 3) we obtained the three parameters: mean crystallite size $L = 5.1$ nm, mean strain $\sigma = 530$ N mm^{-2}, and mean stacking fault probability $\alpha = 5.0\%$. The corresponding values for the $Pt_{50}Au_{50}$ sample are 3.6 nm, 550 N mm^{-2}, and $\alpha = 2.5\%$.

The observed lattice parameters related to the peak positions are $a = 0.4035$ nm, and $a = 0.4010$ nm for $Pt_{20}Au_{80}$ and $Pt_{50}Au_{50}$, respectively. Figure 4 shows a diagram of *a* versus

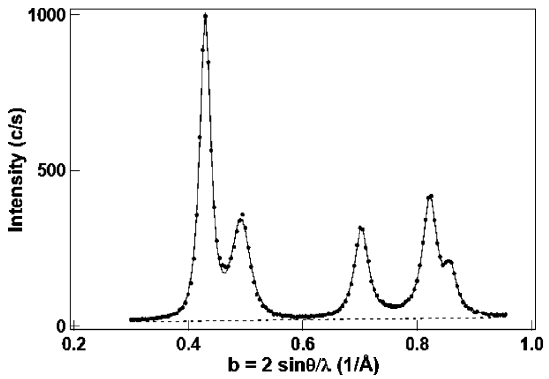

Figure 2. WAXS diffractograms of $Pt_{20}Au_{80}$ alloy catalyst (40 wt % metal loading) prepared by w/o microemulsion. Experimental points are represented by dots. Solid line shows the diffraction line profile fitting.

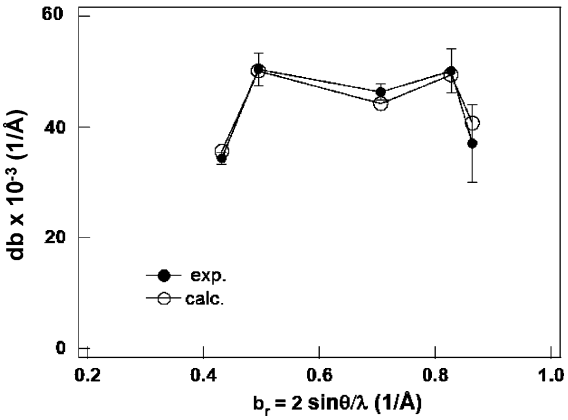

Figure 3. Analysis of the integral line width, *db*, as a function of the peak positions, b_r.

Au concentration for the known values for the bulk Pt−Au system,[39] compared with the measured *a*-values, assuming the nominal Au concentration of 50 and 80 at. %. There is a striking deviation from the nominal 50% Au concentration to an apparently higher Au content of ∼65 at. %, whereas the *a*-parameter of $Pt_{20}Au_{80}$ -sample fits the bulk data. Such apparently higher Au content can be alternatively explained by an enrichment of Au atoms in the core, and segregation of the smaller Pt atoms to the particle surface. Model calculations for another bimetallic Pt−Ru system have shown that segregation effects do, in fact, modify the net lattice spacing observed in an XRD diagram.[40]

Electrochemical Characterization

Surface Composition. Surface composition of catalysts have been determined using cyclic voltammetry in alkaline medium (0.1 M NaOH). Figure 5 shows cyclic voltammograms of $Pt_{50}Au_{50}$/C and $Pt_{20}Au_{80}$/C catalysts. All the current values were normalized with the active surface area of the electrodes.

The charge associated with the reduction of oxide species of the electrode surface can be used to determine the surface composition.[41] The peak around −0.38 V versus MSE during negative sweep is associated with gold species, whereas the one at −0.8 V versus MSE corresponds to platinum species. For pure catalysts, with an upper potential limit of +0.25 V versus MSE, the charge values of 493 and 543 μC cm^{-2} were obtained for Pt and Au, respectively.

The atomic content of the Pt−Au nanoparticles can be deduced as follows:

$$x = \frac{S_{Au}}{S_{Au} + S_{Pt}} \times 100$$

where *x* represents the Au content, and S_{Au} and S_{Pt} are the electrode surface covered by gold and platinum oxides, respectively. The different results obtained from characterization of synthesized particles are summarized in Table 1. The Au content of 74.1% in the surface composition of $Pt_{20}Au_{80}$ catalyst is estimated, while the Au content in $Pt_{50}Au_{50}$ is 18.4%. The striking difference on the surface composition suggests an enhanced segregation effect of Pt, which is favored in $Pt_{50}Au_{50}$. The anomalous large lattice spacing of this material, observed by XRD, strongly supports the surface segregation of platinum.[40]

Glucose Oxidation. The reactivity of catalysts versus glucose oxidation were studied using cyclic voltammetry in phosphate buffer at pH 7. The voltammograms for Pt, Au and Pt−Au alloy nanoparticles in phosphate buffer (pH 7.0) in the presence of

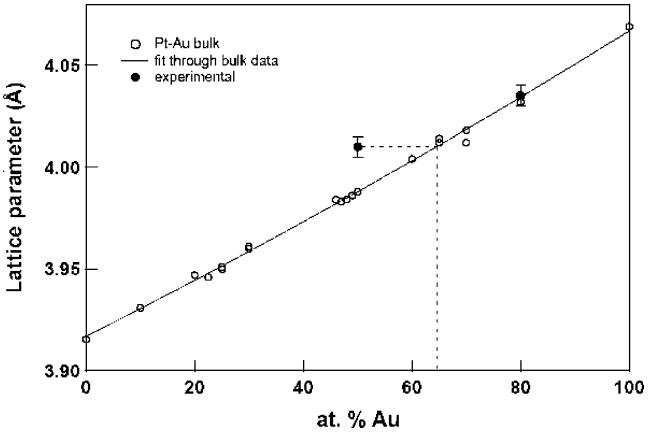

Figure 4. Experimental lattice parameters of the $Pt_{50}Au_{50}$ and $Pt_{20}Au_{80}$ alloy nanoparticles compared with literature data for bulk Pt−Au alloys obtained by Darling et al.[39] (small circles).

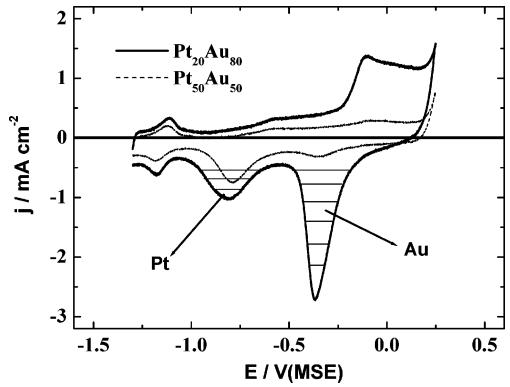

Figure 5. Cyclic voltammograms of Pt−Au alloy nanoparticles deposited on carbon disk electrode recorded in 0.1 M NaOH at 20 mV s^{-1} and at 25 °C. The horizontal segments denote the region considered for the evaluation of the surface composition.

0.1 M D-glucose are given in Figure 6. For Pt and $Pt_{50}Au_{50}$ (Figure 6a), three oxidation peaks (A, B, and C) occur during the positive potential sweep, whereas three other peaks (D, E, and F) are observed during the negative going scan. At low potentials (in the so-called hydrogen region), the peak A was attributed by many authors to dehydrogenation of the anomeric carbon on platinum.[18−20] The peaks B and C, observed in the so-called gold and platinum hydroxides region, correspond to the direct oxidation of glucose. On the $Pt_{20}Au_{80}$ catalyst, the different oxidation peaks are not well defined (Figure 6b). The presence of Pt content at 20% contributes to the glucose oxidation, which starts earlier than that on Au alone. It can be noticed that dehydrogenation of glucose at the anomeric carbon in C_1 position on the Pt surface occurs at −1 V versus MSE. This oxidation process continues by a large shoulder until the formation of the oxidation peak B′ at the Au−OH sites. The oxidation of glucose on the gold hydroxide is well visible in Figure 6b (peaks G and H). During the negative going scan and after the reduction of hydroxides on $Pt_{20}Au_{80}$, a new oxidation takes place by the presence of peaks D and E. It can be noticed that glucose electrooxidation occurs in three potential regions: the first region is in the potential range as for pure platinum, whereas the second one is in the same potential range as pure gold. The third region is located between Pt−OH and Au−OH formations which contribute to enhance the reaction by a synergistic effect of the alloy material. As a result, the presence of platinum in the alloy favors the dehydrogenation of glucose and gold allows to increase the current densities as shown by Möller and Pistorius.[42] Blank measurements in the same time interval only reflect the effect of double layer charging (t < 1 ms).

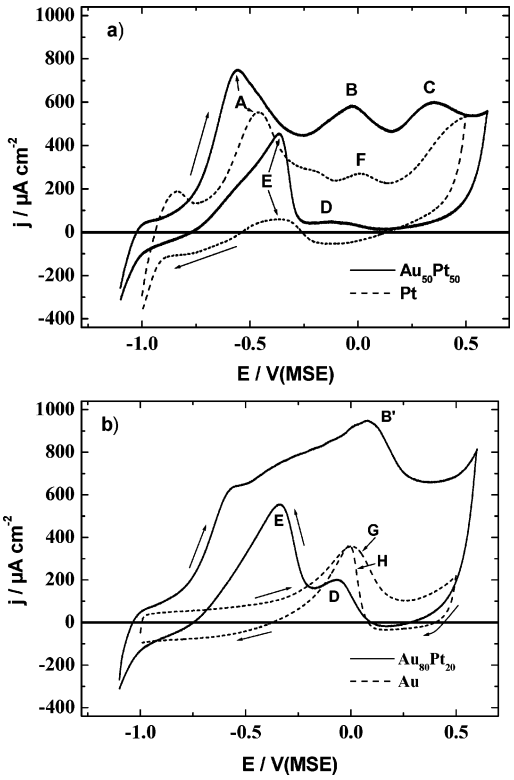

Figure 6. Cyclic voltammograms of Pt, Au, and Pt−Au alloy nanoparticles deposited on carbon rotating disk electrode recorded in phosphate buffer (pH 7.0) in the presence of 0.1 M glucose at 20 mV s^{-1} and 25 °C.

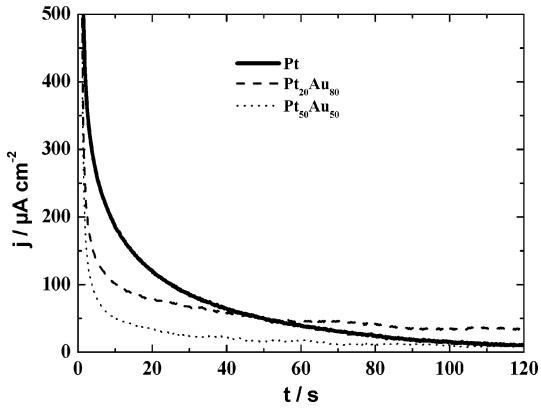

Figure 7. Polarization current vs time plots for the electrooxidation of glucose in phosphate buffer (pH 7.0) at −0.65 V vs MSE.

The performances of these electrocatalysts to oxidize glucose have been evaluated via chronoamperometric experiments carried out at −0.65 V versus MSE for the platinum and Pt−Au alloy nanoparticles (Figure 7). In the case of $Pt_{20}Au_{80}$ alloy, the presence of gold particles allows the enhancement of the activity as compared to platinum for a time superior to 60 s.

Fuel Cell Test. The feasibility of a biofuel cell (BFC) which associates the bimetallic anode ($Pt_{20}Au_{80}$) and a biocathode has been evaluated (Figure 8). For the biocathode, both enzyme and mediator were co-immobilized on the external surface of the tube by their entrapment in the polymer such as polypyrrole. Entrapment occurs during the electropolymerization carried out by controlled potential electrolysis in the presence of both the monomers and the biomolecules in solution.[43] Glucose oxidation was performed by the bimetallic catalyst at the anode, whereas

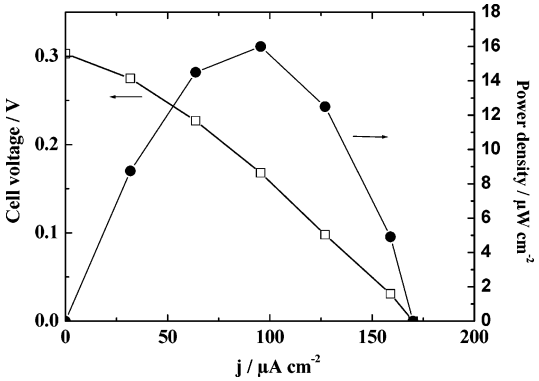

Figure 8. Performance of glucose/O_2 fuel cell using $Pt_{20}Au_{80}$ anode and biocathode (ABTS+Laccase 27 mU cm^{-2}) in phosphate buffer (pH 5.0) at 37 °C. (a) Cell voltage vs current density; (b) power density vs current density.

oxygen was reduced by laccase co-immobilized with 2,2′-azinobis (3-ethylbenzothiazoline-6-sulfonate) diammonium salt ($ABTS^{2-}$) at the cathode. The electrodes were soaked in a glucose solution (0.1 M) saturated with nitrogen gas. An O_2 saturated liquid-phase circulated through a porous carbon tube used as the biocathode and oxygen diffuser. The inside of the cathode tube was continuously supplied by oxygen saturated solution that was likely to diffuse from the inner surface to the external one of the porous tube. The BFC prototype used in this work was recently described.[14] Figure 8 shows the power density and the cell voltage as a function of current density. The maximum power density of the fuel cell is 16 μW cm^{-2} at 0.16 V and 100 μA cm^{-2}. The low open circuit voltage (0.3V) is essentially due to the loss at the cathode. Considering that glucose oxidation takes place at 0.1 V versus RHE and that of O_2 reduction on a Pt electrode at 0.8 V versus RHE, the expected open circuit voltage (OCV) should be close to 0.7 V. However, the OCV determined by linear polarization curves for anode and cathode electrodes, in hemi-cells, was ca. 0.4 V, which is also far from 0.7 V. This difference can be explained by the slow equilibrium of adsorption/desorption processes and coverage at the anode catalyst surface. On the other hand, the reversible potential also depends on the nature of the mediator in the cathodic compartment.

Conclusion

Nanoscale Pt−Au alloy catalysts were synthesized by w/o microemulsion to use them as anodes for glucose oxidation. Physicochemical characterizations (WAXS and TEM) of the alloy nanoparticles were correlated with those obtained by electrochemical measurements for $Pt_{20}Au_{80}$ catalyst. The obtained Au−Pt catalysts display electrocatalytic activity with respect to glucose oxidation as evidenced by cyclic voltammetry and chronoamperometry. To some extent, the electrical efficiency obtained with the bimetallic composition can be explained by the stability of both its surface composition and the bulk material. As a result Pt−Au alloy nanoparticles enhanced the activity of the electrode material, which favored the dehydrogenation of glucose at the anomeric carbon. To improve the electrical performance of this biofuel cell, two main parameters must be taken into account: (i) the optimization of the nominal surface composition of the Pt−Au alloy catalysts, (ii) the decrease of glucose concentration lower than 10 mM with respect to medical applications.

Acknowledgment. The authors acknowledge "le Conseil Régional de Poitou-Charentes" for financial support of this project. N. Alonso-Vante expresses his thanks to the Alexander von Humboldt Stiftung and the Max-Planck-Society for funding his stay at the Fritz-Haber-Institut.

References and Notes

(1) Heller, A. *Phys. Chem. Chem. Phys.* **2004**, *6*, 209.
(2) Katz, E.; Willner, I.; Kotlyar, A. B. *J. Electroanal. Chem.* **1999**, *479*, 64.
(3) Palmore, G. T. R.; Kim, H.-H. *J. Electroanal. Chem.* **1999**, *464*, 110.
(4) Ikeda, T.; Kano, K. *J. Biosci. Bioeng.* **2001**, *92*, 9.
(5) Chen, T.; Barton, S. C.; Binyamin, G.; Gao, Z.; Zhang, Y., Kim, H.-H.; Heller, A. *J. Am. Chem. Soc.* **2001**, *123*, 8630.
(6) Tsujimura, S.; Tatsumi, H.; Ogawa, J.; Shimizu, S.; Kano, K.; Ikeda, T. *J. Electroanal. Chem.* **2001**, *496*, 69.
(7) Kim, H.-H.; Mano, N.; Zhang, Y.; Heller, A. *J. Electrochem. Soc.* **2003**, *150*, A209.
(8) Mano, N.; Mao, F.; Heller, A. *J. Am. Chem. Soc.* **2003**, *125*, 6588.
(9) Mano, N.; Mao, F.; Heller, A. *J. Electroanal. Chem.* **2005**, *574*, 347.
(10) Farneth, E.; D'Amore, M. B. *J. Electroanal. Chem.* **2005**, *581*, 197.
(11) Liu, Y.; Wang, M.; Zhao, F.; Liu, B.; Dong, S. *Chem. Eur. J.* **2005**, *11*, 4970.
(12) Barrière, F.; Kavanagh, P.; Leech, D. *Electrochim. Acta* **2006**, *51*, 5187.
(13) Bullen, R. A.; Arnot, T. C.; Lakeman, J. B.; Walsh, F. C. *Biosens. Bioelectron.* **2006**, *21*, 2015.
(14) Brunel, L.; Denele, J.; Servat, K.; Kokoh, K. B.; Jolivalt, C.; Innocent, C.; Cretin, M.; Rolland, M.; Tingry, S. *Electrochem. Commun.* **2007**, *9*, 331.
(15) Farneth, E.; Diner, B. A.; Gierke, T. D.; D'Amore, M. B. *J. Electroanal. Chem.* **2005**, *581*, 190.
(16) Ramanavicius, A.; Kausaite, T. A.; Ramanaviciene, A. *Biosens. Bioelectron.* **2005**, *20*, 1962.
(17) Kang, C.; Shin, H.; Heller, A. *Bioelectrochem.* **2005**, *68*, 22.
(18) Ernst, S.; Heitbaum, J.; Hamann, C. H. *J. Electroanal. Chem.* **1979**, *100*, 173.
(19) Ernst, S.; Heitbaum, J.; Hamann, C. H. *Ber. Bunsen-Ges. Phys. Chem.* **1980**, *84*, 50.
(20) Essis Yei, L. H.; Beden, B.; Lamy, C. *J. Electroanal. Chem.* **1988**, *246*, 349.
(21) Kokoh, K. B.; Léger, J.-M.; Beden, B.; Lamy, C. *Electrochim. Acta* **1992**, *37*, 1333.
(22) Kokoh, K. B.; Léger, J.-M.; Beden, B.; Huser, H.; Lamy, C. *Electrochim. Acta* **1992**, *37*, 1909.
(23) Largeaud, F.; Kokoh, K. B.; Beden, B.; Lamy, C. *J. Electroanal. Chem.* **1995**, *397*, 261.
(24) Wu, M. L.; Chen, D. H.; Huang, T. C. *Chem. Mater.* **2001**, *13*, 599.
(25) Capek, I. *Adv. Colloid Int. Sci.* **2004**, *110*, 49.
(26) Lopez-Quintela, M. A. *Curr. Opin. Interface Sci.* **2003**, *8*, 137.
(27) Hernandez, J.; Solla-Gullon, J.; Herrero, E. *J. Electroanal. Chem.* **2004**, *574*, 185.
(28) Eriksson, S.; Nylén, U.; Rojas, S.; Boutonnet, M. *Appl. Catal. A: Gen.* **2004**, *265*, 207.
(29) Luo, J.; Maye, M. M.; Petkov, V.; Kariuki, N. N.; Wang, L.; Njoki, P.; Mott, D.; Lin, Y.; Zhong, C.-J. *Chem. Mater.* **2005**, *17*, 3086.
(30) Santos, L. G. R. A.; Oliveira, C. H. F.; Moraes, I. R.; Ticianelli, E. A. *J. Electroanal. Chem.* **2006**, *596*, 141.
(31) Slot, J. W.; Geuze, H. J. *Eur. J. Cell Biol.* **1985**, *38*, 87.
(32) Pileni, M. P. *Langmuir* **1997**, *13*, 3266.
(33) (a) Gnutzmann, V.; Vogel, W. *J. Phys. Chem.* **1990**, *94*, 4991. (b) Vogel, W. *Cryst. Res. Technol.* **1998**, *33*, 1141.
(34) Bonnemann, H.; Braun, G.; Brijoux, W.; Brinkmann, R.; Tilling, A. S.; Seevogel, K.; Siepen, K. *J. Organometallic Chem.* **1996**, *520*, 143.
(35) Williamson, G. K.; Hall, W. H. *Acta Metall.* **1953**, *1*, 22.
(36) Warren, B. E. *X-Ray Diffraction*; Addison-Wesley: Reading, MA, 1969; p 275.
(37) Vogel, W.; Tesche, B.; Schulze, W. *Chem. Phys.* **1983**, *74*, 137.
(38) Vogel, W.; Bradley, J.; Vollmer, O.; Abraham, I. *J. Phys. Chem. B* **1998**, *102*, 10853.
(39) Darling, A. S.; Mintern, R. A.; Chaston, J. C. *J. Inst. Met.* **1952−53**, *81*, 125.
(40) Vogel, W.; Britz, P.; Boennemann, H.; Rothe, J.; Hormes, J. *J. Phys. Chem. B* **1997**, *101*, 11029.
(41) Burke, L. D.; Moran, J. M.; Nugent, P. F. *J. Solid State Electrochem.* **2003**, *7*, 529.
(42) Möller, H.; Pistorius, P. C. *J. Electroanal. Chem.* **2004**, *570*, 243.
(43) Servat, K.; Tingry, S.; Brunel, L.; Querelle, S.; Cretin, M.; Innocent, C.; Jolivalt, C.; Rolland, M. *J. Appl. Electrochem.* **2006**, *37*, 121.